Two-dimensional Monte Carlo simulations of coarse-grained poly(3-hexylthiophene) (P3HT) adsorbed on striped substrates

Nicolai Oberthür, Jonathan Gross, and Wolfhard Janke

Citation: The Journal of Chemical Physics **149**, 144903 (2018); doi: 10.1063/1.5046383
View online: https://doi.org/10.1063/1.5046383
View Table of Contents: http://aip.scitation.org/toc/jcp/149/14
Published by the American Institute of Physics

Two-dimensional Monte Carlo simulations of coarse-grained poly(3-hexylthiophene) (P3HT) adsorbed on striped substrates

Nicolai Oberthür,[a] Jonathan Gross,[b] and Wolfhard Janke[c]
Institut für Theoretische Physik, Universität Leipzig, Postfach 100 920, 04009 Leipzig, Germany

(Received 27 June 2018; accepted 17 September 2018; published online 12 October 2018)

We investigate the structural phases of single poly(3-hexylthiophene) (P3HT) polymers that are adsorbed on a two-dimensional substrate with a striped pattern. We use a coarse-grained representation of the polymer and sophisticated Monte Carlo techniques such as a parallelized replica exchange scheme and local as well as non-local updates to the polymer's configuration. From peaks in the canonically derived observables, it is possible to obtain structural phase diagrams for varying substrate parameters. We find that the shape of the stripe pattern has a substantial effect on the obtained configurations of the polymer and can be tailored to promote either more stretched out or more compact configurations. In the compact phases, we observe different structural motifs, such as hairpins, double-hairpins, and interlocking "zipper" states. *Published by AIP Publishing.*
https://doi.org/10.1063/1.5046383

I. INTRODUCTION

Ever since the thermodynamic properties of single polymers in solution have been generally understood, people began to investigate the effects of the presence of attractive substrates. Since a homogeneous substrate cannot have much variation, researchers were interested in patterned substrates and the ability of polymers to recognize these patterns. Recent studies have looked at these kinds of systems with abstract models via computer simulations.[1–7]

One polymer of particular interest in recent years is regioregular poly(3-hexylthiophene) (P3HT) due to its semiconductive properties.[8–11] It has the potential to be used in low-cost, flexible organic solar cells.[12–14] Because any electronic device needs to have some sort of boundary for the polymer melt and because the active layer of organic solar cells gets manufactured thinner and thinner, it is of high interest to study the behavior of P3HT in the vicinity of a substrate. Many experiments of adsorbed P3HT have been conducted, but they were limited by the number of available substrates.[15–18]

Building up on the study by Förster *et al.*,[18] who investigated P3HT adsorbed on a Au(001) substrate in an ultrahigh vacuum at room temperature, we work to get a thorough understanding of the behavior of a single poly(3-hexylthiophene) molecule on a structured substrate. We employ sophisticated Monte Carlo (MC) simulations of a coarse-grained P3HT chain on an abstract surface in two dimensions. This approach was chosen to explicitly investigate adsorbed polymers because Förster *et al.* found that in both experiment and simulation, the polymers did almost never desorb from the substrate under the given physical conditions. We implement the coarse-grained P3HT model that was developed by Huang *et al.*[19] and introduce a two-dimensional substrate model with an attractive stripe pattern, which is motivated by the Au(001) surface reconstruction.[20] We use parameters that resemble the stripe distance of the Au(001) pattern as well as stripes that are closer together. With this approach, it is possible to modulate the substrate-interaction parameter in a systematic way in order to identify the structural phases of the polymer. This information can then be organized into structural phase diagrams, which give deep insight into the influence of the substrate on the polymer.

The rest of this paper is organized as follows. In Sec. II, an explanation of the coarse-grained polymer model as well as the substrate model will be given. Additionally, the Monte Carlo methods will be presented. The results as well as an in-depth discussion for short and long polymers will be provided in Sec. III. Finally the paper will be concluded in Sec. IV.

II. MODEL AND METHODS

A. Coarse-grained polymer model

In order to produce results for long polymers in reasonable computing times, a coarse-grained model of regioregular P3HT was implemented. The model, which was derived by Huang *et al.*,[19] consists of three types of particles: The thiophene ring makes up the backbone particles, denoted as P1; the inner part of the side chain with the first three methyl groups, denoted as P2; and the second part of the side chain with the outer three methyl groups, denoted as P3. The coarse-grained particles and their relation to the atomistic representation of the P3HT are displayed in Fig. 1.

There are four contributions to the internal energy U_{int} of the coarse-grained polymer model: Interaction of bonded particles U_{bond}, a bending energy of the angles between two

[a]oberthuer@itp.uni-leipzig.de
[b]gross@itp.uni-leipzig.de
[c]janke@itp.uni-leipzig.de

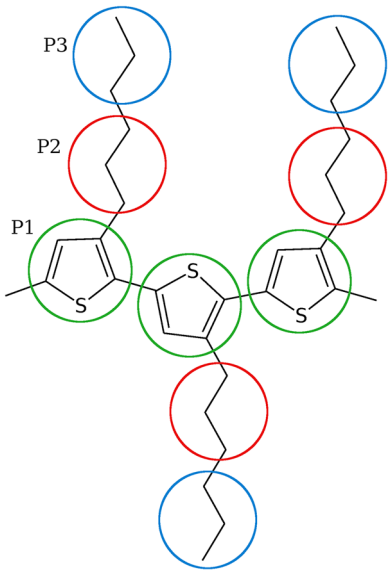

FIG. 1. Visualization of the coarse-grained particles in relation to the chemical structure of P3HT. The backbone and side-chain atoms are grouped into "super atoms" that lie on the center of mass of the thiophene ring (P1), the first three methyl groups from the side chain (P2), and the outer three methyl groups (P3). Reproduced with permission from Förster *et al.*, J. Chem. Phys. **141**, 164701 (2014). Copyright 2014 AIP Publishing LLC.

bonds U_{bend}, a torsion potential of dihedral planes U_{dihed}, and the interaction of non-bonded particles U_{nonbond}. Two bonded particles with a distance d will interact according to the power series

$$U^*_{\text{bond}}(d) = \sum_{i=2}^{n} c_i (d - d_0)^i, \tag{1}$$

where the parameters c_i and d_0 are different for the various bond types P1-P1, P1-P2, and P2-P3. The parameters are given in the supplementary material of Ref. 19. The equilibrium distances d_0 are compiled in Table I for easier reference. The formula in Eq. (1) just gives the contribution of a single bond. Summing up all the contributions, U^*_{bond} for every single bond in the chain will give the full bond potential energy $U_{\text{bond}} = \sum_{\text{bonds}} U^*_{\text{bond}}$.

The bending energy is also given by a power series, but this time in terms of the angle ϕ between a pair of bonds,

$$U^*_{\text{bend}}(\phi) = \sum_{i=0}^{n} c_i (\phi - \phi_0)^i. \tag{2}$$

Again the parameters c_i and ϕ_0 differ for the four distinct angle types between the various kinds of coarse-grained particles and are given in the supplementary material of Ref. 19. As above, the star in U^*_{bend} refers to the fact that this is the contribution of a single angle and all the angles have to be summed up to obtain the full potential energy U_{bend}. Both the angle along the backbone (P1-P1-P1) and the angle within the side chains (P1-P2-P3) are symmetrical around an angle of $\phi = 180°$ with the minima of the backbone bending potential at $\phi \approx 165°$ and $\phi \approx 195°$ and minima of the side-chain angle at $\phi \approx 160°$ and $\phi \approx 200°$. Due to the regioregular head-to-tail coupling of the underlying atomistic structure of the considered P3HT, the angles between P1-P1-P2 and P2-P1-P1 have to be distinguished. The bending potential of the P1-P1-P2 angle has a minimum at $\phi \approx 122°$, and the potential of the P2-P1-P1 angle at $\phi \approx 83°$.

The dihedral angle θ that enters the torsion potential is the angle between the normal vectors of two planes which are spanned by the bonded particles A-B-C and B-C-D. In Ref. 19, the torsion potential is given by a series of cosine powers. However, in the case of two-dimensional (2D) simulations, only two cases can occur: planes can either be parallel or anti-parallel. In the parallel case, the normal vectors point in the same direction, which corresponds to a dihedral angle of $\theta = 0°$. The normal vectors of anti-parallel planes point in the opposite direction and have a dihedral angle of $\theta = 180°$. The values for both 2D-cases were extracted from the potentials given in Ref. 19 and are displayed in Table II. The most notable effect of the torsion potential comes from the P2-P1-P1-P2 part. It favors configurations where consecutive side chains are on the opposite sides of the backbone, the so called trans-configuration. The model by Huang *et al.*[19] also features an improper dihedral potential $U_{\text{improp}}(\psi)$ of the nonbonded P1-P2-P1-P1 particles, which was not included in this work because it produces unreasonably high values for the angles of $\psi = 180°$.

Finally, there are interactions U_{nonbond}, which model Lennard-Jones and Coulomb interactions between particles that are not bonded in the polymer. This potential is given in tabular form in the supplementary material of Ref. 19. The table stores the numerical values (in units of kcal/mol) of this interaction as a function of the distance d between two nonbonded particles for the six possible combinations of particle types. This potential is displayed in Fig. 2.

The full potential energy of the model of this study $U_{\text{pot}} = U_{\text{int}} + U_{\text{sub}}$ also takes the interaction between the polymer and the substrate into account, which will be described in Subsection II B.

B. 2D substrate model

A simulation in two dimensions can be seen as a model for a system where the polymer is adsorbed on a homogeneous flat

TABLE I. Equilibrium distances d_0 of the different bond types.

Bond type	d_0 (Å)
P1-P1	3.8283
P1-P2	4.0717
P2-P3	3.5379

TABLE II. Values of the torsion potential U^*_{dihed} for the different types of dihedrals in the two possible configurations.

	$U^*_{\text{dihed}}(\theta)$ (kcal/mol)	
Dihedral type	$\theta = 0°$	$\theta = 180°$
P1-P1-P1-P1	0	0.7419
P2-P1-P1-P2	0.8144	0
P1-P1-P2-P3	0.028	0.671
P3-P2-P1-P1	0.6656	0.225

substrate. Natural surfaces of crystals can exhibit more complex structures due to the reconstructions of the crystal lattices in the outermost layers.[18,20] Such a reconstruction is also found on the Au(001) surface and leads to height modulations that form a striped pattern.[20] The stripes run along the [110] direction of the bulk fcc lattice. This modulation has a wavelength of $\lambda \approx 13.85$ Å and an amplitude of $\Delta h \approx 0.7$ Å.[18]

The simulations in Ref. 18 used a cosine shape that stretched over the wavelength λ of the Au(001) reconstruction pattern. However, the amplitude $\Delta h \approx 0.7$ Å is only very small compared to the wavelength $\lambda \approx 13.85$ Å. This led to a polymer that did not react to the stripe pattern very much.

So in order to make the effects of the stripes more visible and, also, because height modulations of the substrate are not possible in 2D, a different approach was taken for this work. A substrate potential energy was introduced that features attractive stripes and plateaus in between the stripes that do not interact with the polymer. The substrate is modelled by a periodic function in the y-direction of the simulation's coordinate system. In this model, only the backbone of the polymer interacts with the substrate, whereas the side chains do not. This is motivated by the fact that the sulfur atom of the thiophene ring has the strongest bond with the gold atoms from the substrate, whereas carbon and hydrogen interact much weaker. For a backbone particle with coordinates $\vec{r} = (x, y)$, the potential is given by

$$U^*_{\text{sub}}(y) = \begin{cases} 0, & \text{between stripes,} \\ -\varepsilon f_{\text{stripe}}(y), & \text{inside stripes,} \end{cases} \tag{3}$$

$$f_{\text{stripe}}(y) = \frac{1}{2}\left[\cos\left(\pi \frac{y}{r_{\text{Au}}}\right) + 1\right]. \tag{4}$$

For backbone particles inside a stripe, the potential energy has a cosine shaped valley given by f_{stripe}. Between two stripes, the potential is constant at zero. The interaction strength ε (in units of kcal/mol) determines the depth of the valleys in the potential and, thus, how strongly the polymer can interact with the stripes. The distance between two minima of the potential, i.e., the distance of two stripes D_{stripe}, is given by $D_{\text{stripe}} = m \times d_0$, where $d_0 = 3.8283$ Å denotes the equilibrium distance of the P1-P1 bond between two backbone particles and m is a multiplier. This stripe-distance parameter m can be seen as the stripe distance in units of the P1-P1 equilibrium bond distance and is the parameter that was actually varied during the study along with the interaction parameter ε. The parameter $r_{\text{Au}} = 1.35$ Å was chosen according to Ref. 21 as the atomic radius of gold in a crystal and corresponds to half of the width of the valleys. It was kept at this fixed value throughout the whole study. A plot of the substrate potential energy is given in Fig. 3 for a substrate with interaction strength $\varepsilon = 0.5$ kcal/mol and stripe-distance parameter $m = 2$.

C. Monte Carlo methods

Monte Carlo (MC) simulations are a method to access the thermodynamic behavior of a system by statistical means.[22–24] Instead of solving the equations of motion for all the particles as done in Molecular Dynamics (MD) studies, a sample of states is drawn from a thermodynamic ensemble. Each state that gets drawn is only dependent on the state that was drawn immediately before. This can be seen as a random walk in the phase space of the system. If the sample states are drawn according to the underlying probability distribution, ensemble averages can be estimated from the observable values in the sample states: For M sample states, an estimator of the expectation value is given by $\langle \mathcal{O} \rangle \approx \overline{\mathcal{O}} = (1/M) \sum_{i=1}^{M} \mathcal{O}_i$.

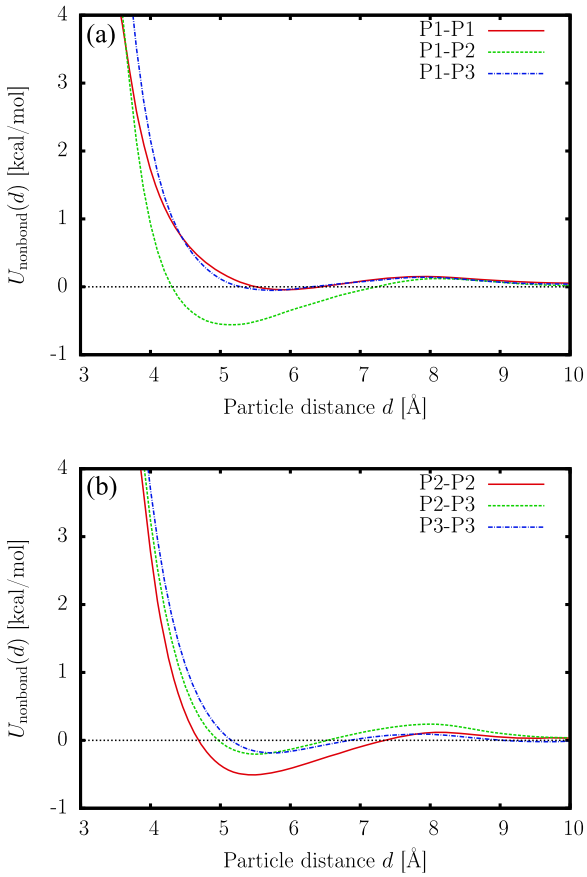

FIG. 2. Shape of the potential of the non-bonded interactions $U_{\text{nonbond}}(d)$ in terms of the particle distance d for the backbone (a) and side chains (b) of the polymer. All the potentials feature an attractive minimum and a repulsive maximum.

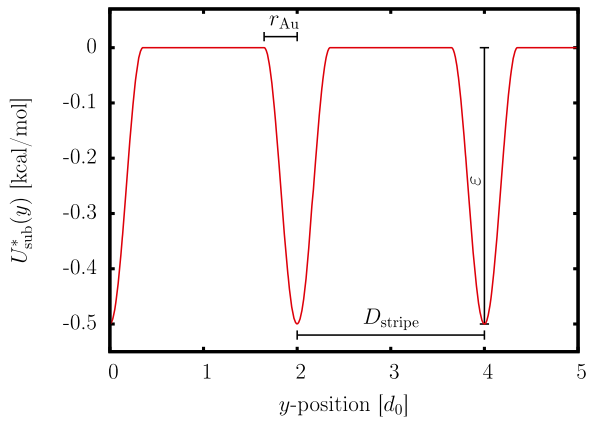

FIG. 3. Plot of the substrate potential energy $U^*_{\text{sub}}(y)$ for a substrate with interaction strength $\varepsilon = 0.5$ kcal/mol and distance parameter $m = 2$. Note that the y-coordinate is already measured in units of the equilibrium bond distance d_0 of the P1-P1 bond potential.

The sampling for this study was done with the Metropolis algorithm[25,26] and the replica exchange parallel tempering[27–30] scheme. The Metropolis algorithm takes a polymer configuration ω and applies a random update proposal to it, putting it into a configuration ω'. Then the canonical weights of both states are compared, and the update either gets accepted or rejected according to $p_{\text{update}}(\omega \to \omega') = \min(1, \exp(-\beta \Delta E))$, where $\beta = 1/k_B T$ is the inverse temperature with Boltzmann's constant k_B and $\Delta E = E(\omega') - E(\omega)$ is the energy difference between the two states.

Several random update moves for the Metropolis algorithm were implemented. The simplest one is a single particle shift: A random particle gets chosen and is shifted along a random displacement vector to new coordinates. This type of update can be compared to a "realistic" particle motion by thermal fluctuations. In order to achieve a better sampling of the phase space, more intricate update moves were implemented as well. Two-dimensional pivot rotations[31,32] rotate either a part of the backbone or a side chain by a random angle around a rotation axis. This axis is situated at a random backbone particle and is oriented perpendicular to the simulation plane. During the thermalisation of the system, the maximum rotation angles as well as the maximum displacement vector are tuned to achieve a desired acceptance rate of their respective updates. The desired acceptance rate was chosen to be 25%. Additional updates are a slithering snake move[33,34] and a side-chain flip update. During the slithering snake move, the first or last repeat unit of the polymer gets "cut off" from the chain and is then "glued" back onto the other end. Randomly the first or last backbone bond of the chain gets chosen. The bond is then severed, and the repeat unit that was cut off gets shifted to the other end of the polymer, where it is reattached to the chain by a new bond that has the same length and angle regarding the simulation's coordinate system as the severed bond. Finally, the side-chain flip update takes a random repeat unit and flips its side chain to the other side of the backbone. Without this update, it would be impossible to sample the entire phase space in two dimensions because otherwise side chains could only cross to the other side of the backbone at the ends of the polymer. After a number of update attempts that equal the number of particles in the chain, which is called an update sweep, the polymer gets translated back to the origin of the simulation coordinate system, while maintaining its position with regards to the stripes of the substrate. This is done to avoid precision loss in the simulation program for large absolute values of the coordinates.

In addition to the Metropolis sampling, the parallel tempering scheme was implemented. Instead of only investigating a system at a single temperature at a time, several replicas of the system at different temperatures are introduced. The two replicas i and j can exchange their current configurations ω_i and ω_j while keeping their temperatures. The exchange is accepted or rejected according to an acceptance probability $p_{\text{swap}}(\omega_i \leftrightarrow \omega_j) = \min(1, \exp(\Delta\beta\, \Delta E))$, where $\Delta\beta = \beta_i - \beta_j$ and $\Delta E = E(\omega_i) - E(\omega_j)$ denote the differences in inverse temperature and energy between the replicas. This allows configurations from low temperatures to get passed on to higher temperatures, where the increased thermal fluctuations make it possible to overcome barriers in the free-energy landscape. This method also has the great advantage that it can utilize parallel computing, when the replicas are run on different computing nodes, which reduces the necessary wall-clock time of the investigation.

III. RESULTS AND DISCUSSION

In order to investigate the polymer-substrate system of coarse-grained poly(3-hexylthiophene) adsorbed on a striped substrate, parallel tempering Metropolis simulations were carried out. Twenty replicas at temperatures between $T_{\min} = 200$ K and $T_{\max} = 560$ K were set up for each pair of substrate parameters (m, ε). It should be noted that the higher temperatures were chosen from a technical standpoint for the parallel tempering method. The restriction of our model to two dimensions means that no desorption can occur, even though it can be expected that in a three-dimensional study, the polymer would desorb from the substrate at $T < 560$ K. However, as noted above, for temperatures around $T \approx 300$ K, Förster *et al.*[18] observed almost no desorption and, therefore, the two-dimensional approach can be seen as realistic in this range of temperatures.

The distance parameter m was chosen as $m = 2$ and $m = 3.5$. The latter value was motivated by the surface height modulations of the Au(001) surface. As mentioned above, the wavelength of these modulations is $\lambda \approx 13.85$ Å and a value of $m = 3.5$ leads to stripes that are $D_{\text{stripe}} = 13.4$ Å apart. The interaction strength was varied from $\varepsilon = 0$ kcal/mol to $\varepsilon = 2$ kcal/mol in steps of $\Delta\varepsilon = 0.125$ kcal/mol leading to 33 different substrates (for $\varepsilon = 0$, the value of m does not matter). Polymers of $N = 30$ and $N = 65$ repeat units were investigated. The simulation started with 10^6 update sweeps for thermalisation, followed by the production run of 10^7 sweeps. The resulting time series were used to generate the estimators for the observables as well as their canonical derivatives with respect to temperature. In the time series, the two contributions to the energy, i.e., U_{int} from the polymer's internal potential and U_{sub} from the polymer-substrate interaction, were recorded. Additionally the end-to-end distance R_{end} and radius of gyration R_{gyr} were measured. They are given by

$$R_{\text{end}} = |\vec{r}_N - \vec{r}_1|, \tag{5}$$

where $\vec{r}_N, \vec{r}_1$ refer to the positions of the last and the first backbone particle, as well as

$$R_{\text{gyr}} = \left(\frac{1}{3N} \sum_i \left(\vec{r}_i - \vec{\bar{r}} \right)^2 \right)^{1/2}, \tag{6}$$

where the sum runs over all the $3N$ particles of the polymer and $\vec{\bar{r}} = (1/3N) \sum_i \vec{r}_i$.

Structural transitions of the polymer are marked by rapid increases or decreases in the observables. To find the inflection points of the observables, i.e., local extrema in the canonical derivatives (the shorthand $\partial_T \overline{\mathcal{O}} \equiv \partial \overline{\mathcal{O}} / \partial T$ will be used to denote the canonical derivatives in this text), it was necessary to obtain an estimate of the observables and their derivatives at temperatures that were not sampled. This was achieved with the direct multiple-histogram reweighting analysis by Fenwick.[35] This method uses the sampled data from every

replica to get an estimate for the density of states $\tilde{g}(E)$, which can be used to reweight the observable estimators $\overline{\mathcal{O}}$ to any temperature via

$$\overline{\mathcal{O}}(\beta) = \frac{\sum_E \overline{\mathcal{O}}_{\text{micro}}(E)\, \tilde{g}(E) e^{-\beta E}}{\sum_E \tilde{g}(E) e^{-\beta E}}, \tag{7}$$

where the sum runs over all the energy bins that are used to acquire the histograms $H_i(E)$ and $\overline{\mathcal{O}}_{\text{micro}}(E)$ denotes the microcanonical average of the observable in each energy bin. It is computed by taking the average value of the observable for each energy bin in the time series at an inverse temperature β_i,

$$\mathcal{O}_{\text{micro},i}(E) = \frac{\sum_t \mathcal{O}_i(t) \hat{\delta}_{E_i(t),E}}{H_i(E)}, \tag{8}$$

where the sums run over the recorded time series and $\hat{\delta}_{E_i(t),E}$ is reminiscent of the Kronecker delta symbol, i.e., $\hat{\delta}_{E_i(t),E} = 1$ if $E_i(t) \in [E - \Delta E/2, E + \Delta E/2)$ with the histogram bin width ΔE and $\hat{\delta}_{E_i(t),E} = 0$ everywhere else. To get the final microcanonical average $\overline{\mathcal{O}}_{\text{micro}}(E)$, a weighted sum is done over all inverse temperatures β_i.

The reweighted curves are then analyzed for local extrema. Using the techniques from previous studies on flexible and semiflexible polymer adsorption to homogeneous surfaces[36,37] as a template, the positions of these local extrema can subsequently be put into ε–T-diagrams to obtain structural phase diagrams. Error bars were produced with the binning method.[38,39]

A. Short chains with $N = 30$

From the analysis of the reweighted canonical estimators, their derivatives and simulation snapshots we were able to identify several structural phases. For the shorter $N = 30$ polymers, these are characterized by the polymer being either in a compact (C) or an extended (E) configuration. In the compact configurations, the polymer usually forms a structure that resembles a hairpin. The extended configurations are characterized by random-coil states. On the other hand, there is also a distinction whether the polymer aligns itself with the stripes of the substrate (A) or displays no favored direction and lies unaligned on the substrate with a random orientation (U). Additionally, for certain settings of the substrate, one can also observe configurations where the polymer is completely stretched out and aligned to a single stripe (AS). To clarify the terminology, snapshots of the five structural phases are displayed in Fig. 4. They do not represent the most typical states but were instead chosen with the bias to make the distinction of the phases most clear. The findings of the different structural phases were systematized in structural phase diagrams, where the positions of local extrema of the derived observables are displayed. The suggested lines between the peak positions of the derivatives mark the structural transition regions. The derivatives of the measured observables with respect to temperature can be found in Fig. 5.

The phase diagram of a two-dimensional coarse-grained P3HT polymer with $N = 30$ repeat units on a striped surface with the distance parameter $m = 3.5$ for varying attraction of the stripes is displayed in Fig. 6(a). The distance parameter

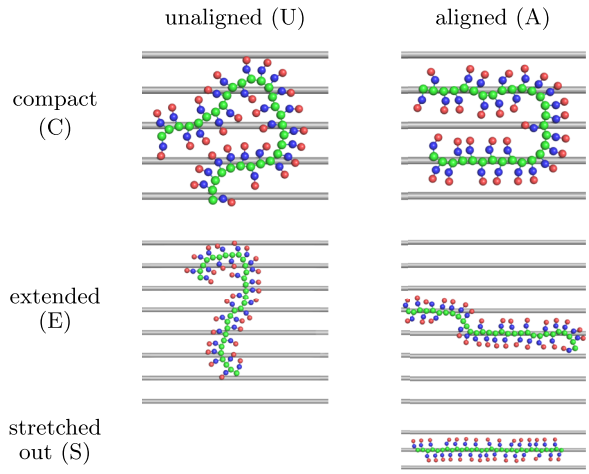

FIG. 4. Snapshots of coarse-grained P3HT polymers of length $N = 30$ in the different structural phases on a substrate with stripe-distance parameter $m = 3.5$. These snapshots represent ideal examples of the different configurations and have been chosen to make the distinction between the structures clear.

value of $m = 3.5$ leads to a substrate that is comparable to the Au(001) surface as mentioned above.

For temperatures $T < 350$ K and weak attraction of the stripes, the polymer is in a collapsed structural phase and it is unaligned with the stripes (UC). By increasing the temperature of the system, one can see more and more microstates where the polymer is extended. A transition to mostly extended states (UE and AE) is marked by local maxima in the derivatives of the end-to-end distance $\partial_T \overline{R}_{\text{end}}$ and radius of gyration $\partial_T \overline{R}_{\text{gyr}}$; cf. Figs. 5(c) and 5(e). The transition temperature of $T \approx 350$ K is mostly unaffected by the interaction strength ε of the stripes up until $\varepsilon \leq 1$ kcal/mol.

In this low-ε region, another transition can be observed. For the weakest polymer-stripe interactions, the polymer will be largely unaligned with the stripes (UC and UE). But with increasing ε, the polymer begins to recognize the stripe pattern and will align itself with them (AC and AE). The transition is marked by local maxima of the substrate specific heat $c_{V,\text{sub}} = (1/N)\partial_T \overline{U}_{\text{sub}}$ that stems from the interaction of the polymer with the substrate. The transition temperatures get shifted up by increasing ε because the energy contribution of the stripes gets more important with increasing ε. The maxima of the substrate specific heat can even be observed in the specific heat of the full system $c_V(T)$ in Fig. 5(a).

For larger values of ε, the polymer's behavior is changed drastically. In the regime of highly attractive stripes with $\varepsilon \geq 1.5$ kcal/mol, the polymer's low-temperature phase is no longer a collection of compact states and instead the polymer is completely stretched out and aligned with a stripe (AS). In this structural phase, hardly any variation in the polymer configuration can be seen. The backbone is stiffly attached to one of the stripes and only the side chains display some small changes in their positions since they are not affected by the substrate potential. At slightly higher temperatures, one can sometimes see a sort of excited state where the polymer is stretched out on two stripes, i.e., it bridges over to a neighboring stripe somewhere along the backbone. As the temperature increases, the polymer becomes more and more "free" from the stripes and

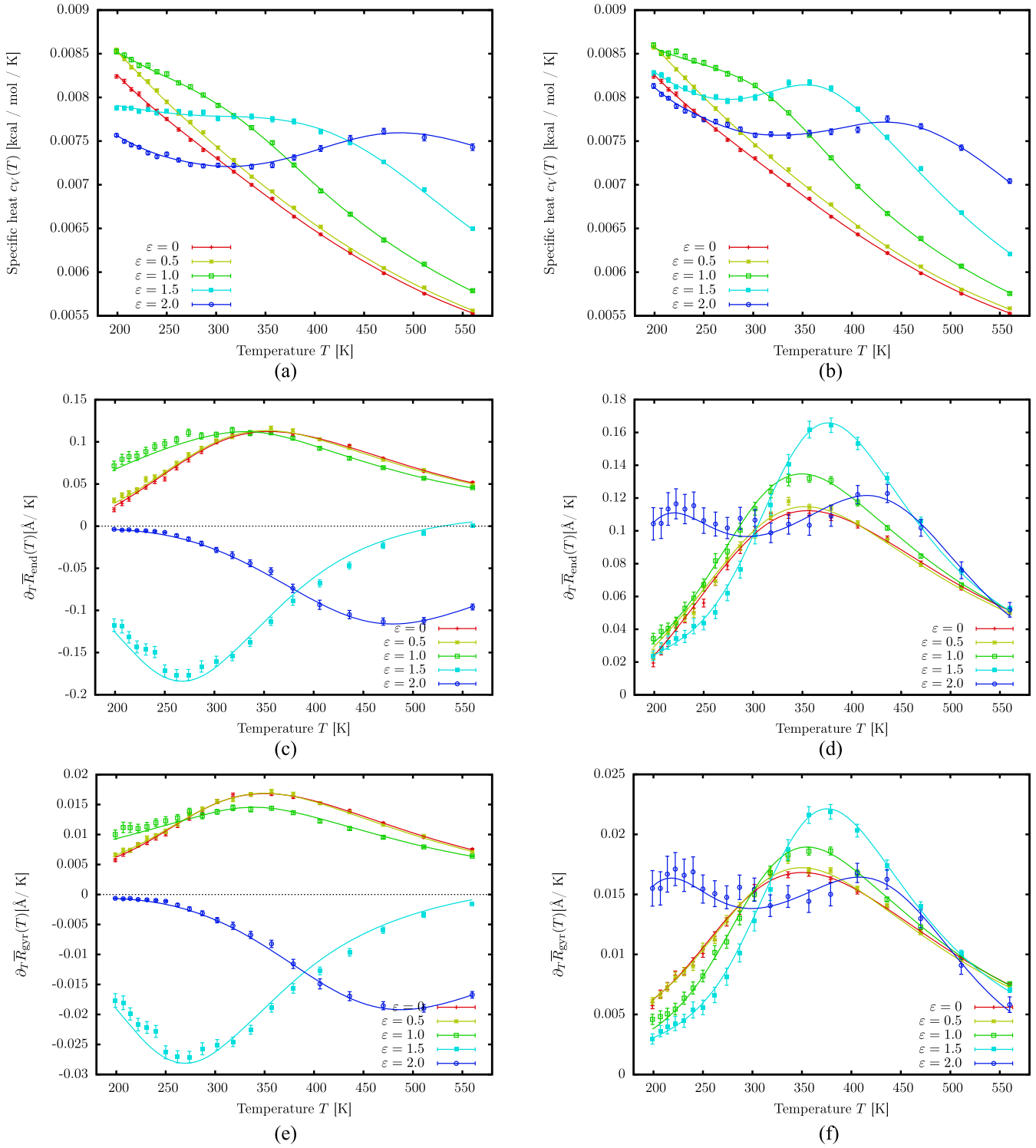

FIG. 5. Derivatives of the various observables for short polymers with $N = 30$ for distance parameter values of $m = 3.5$ [(a), (c), and (e)] and $m = 2$ [(b), (d), and (f)]. Shown are the total specific heat from both internal polymer and substrate interactions $c_V(T)$ [(a) and (b)], the derivatives of the end-to-end distance $\partial_T \overline{R}_{\mathrm{end}}(T)$ [(c) and (d)], and radius of gyration $\partial_T \overline{R}_{\mathrm{end}}(T)$ [(e) and (f)] as functions of temperature T at different values of the interaction parameter ε in units of kcal/mol. The continuous lines between the data points were obtained by the multiple-histogram reweighting.

enters random-coil, extended states (AE). This transition is marked by minima in the derivatives of the end-to-end distance $\partial_T \overline{R}_{\mathrm{end}}$ and radius of gyration $\partial_T \overline{R}_{\mathrm{gyr}}$. Both of these quantities are negative over the whole temperature range, which means that the polymer is shrinking in size with increasing temperatures. This is due to the fact that curly microstates are entropically much more favorable than completely stretched out states. Consequently, this leads to smaller end-to-end distances and radii of gyration in the random-coil phase. For even higher temperatures than the ones considered here, it can be safely assumed that this behavior would change again and $\overline{R}_{\mathrm{end}}$ and $\overline{R}_{\mathrm{gyr}}$ would grow with increasing temperature as is

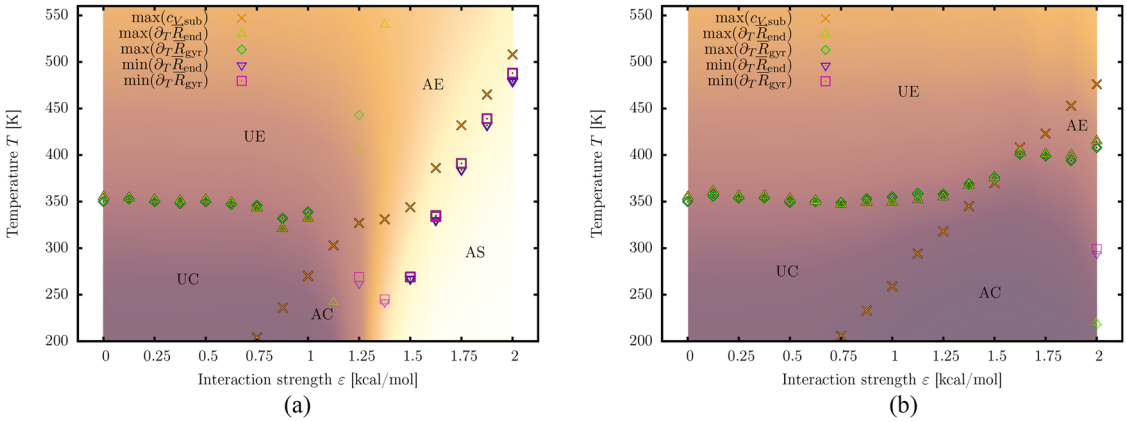

FIG. 6. Structural phase diagram for a polymer of length $N = 30$ and a stripe-distance parameter $m = 3.5$ (a) and $m = 2$ (b). The structural phases are distinguished as extended (E), completely stretched out (S), or compact (C) and as aligned with the stripes of the substrate (A) or unaligned (U). The coloring of the background refers to the end-to-end distance $\overline{R}_{\mathrm{end}}$, where the lowest values are colored in dark purple and the highest values are colored in bright yellow. Both plots use the same range for background color, i.e., the same color refers to the same value in both plots. As such, one can make out several regions that correspond to the compact (C, dark purple), extended (E, brown), and stretched out (S, bright yellow) configurations. Some data points carry less statistical significance and have, therefore, been made fainter as explained in the text.

usually expected in the random-coil phase. In Figs. 5(c) and 5(e), one can see that the curves for $\varepsilon = 1.5$ kcal/mol and $\varepsilon = 2$ kcal/mol begin to approach positive values. The transition is also accompanied by maxima in the substrate specific heat $c_{V,\mathrm{sub}}$ of the polymer-stripe interaction. In contrast to the low-ε region, these maxima here do not point to a transition from aligned to unaligned states because here even for high temperatures, the polymer is still mostly aligned with the stripes. The transition from aligned stretched out configurations to the aligned extended ones is still responsible for a big increase in the energy of the polymer-stripe interaction which results in the maxima of $c_{V,\mathrm{sub}}$ as the polymer "detaches" from the stripes.

In the region where $1.125\ \mathrm{kcal/mol} \leq \varepsilon \leq 1.375\ \mathrm{kcal/mol}$, none of the structural phases can be assigned. Instead, this is the transition region from structures that are mostly dominated by the polymer's internal interactions and entropy to structures where the polymer-stripe interaction becomes most important. Because they do not carry any statistical significance, the measured positions of local extrema of $\partial_T \overline{R}_{\mathrm{end}}$ and $\partial_T \overline{R}_{\mathrm{gyr}}$ in Fig. 6(a) have been made fainter in this region. The $\varepsilon = 1.25$ kcal/mol-system is characterized by the fact that at low temperatures, compact and stretched out microstates occur at the same rate. Additionally, in the histogram of the substrate potential energy U_{sub}, a double peak can be observed for $\varepsilon = 1.375$ kcal/mol. The peaks reflect the stretched out (AS) structures on the one hand and the aligned, compact (AC) structures on the other hand. For higher temperatures, the polymer is mostly in the extended phase but it is not possible to determine where this transition actually takes place, and in this region, the transition from unaligned, extended (UE) to aligned, extended structures (AE) takes place. It might be possible that other observables need to be recorded to see this transition. For this, it could be interesting to find better ways to measure the alignment of the polymer with the stripes. For instance, one could look at the components of the gyration tensor (as demonstrated, for example, in Ref. 40).

In addition to the case of $m = 3.5$, substrates with a stripe-distance parameter of $m = 2$ were studied. The structural phase diagram for the latter substrates can be seen in Fig. 6(b). The low-interaction region $\varepsilon \leq 0.75$ kcal/mol is mostly the same as in the case of $m = 3.5$, which is to be expected because the behavior of the polymer in this region is not dominated by interaction with the substrate anyway. This is also confirmed by Fig. 5. The curves for the low to intermediate interaction strengths $\varepsilon = 0, 0.5, 1$ kcal/mol are almost identical in the left column for $m = 3.5$ to the right column for $m = 2$. Thus, for low temperatures, one again observes an unaligned, compact structural phase (UC) with a transition at $T \approx 350$ K to unaligned, extended states (UE). The systems with slightly stronger attraction parameters $\varepsilon \leq 1$ kcal/mol also look basically the same as before with compact, aligned states (AC) at low temperatures and transitions to compact, unaligned (UC) and finally extended, unaligned (UE) configurations with increasing temperature.

For the more attractive stripes with $\varepsilon \geq 1.25$ kcal/mol, the C $\leftrightarrow$ E transition starts to get shifted up to higher temperatures. The AC configuration is much more dominant on the $m = 2$ substrate than on the $m = 3.5$ one. This happens because on the substrate where the stripes are closer together, the two strands of the hairpin are closer together as well, when the polymer aligns itself with the stripes. This leads to a greater energy reduction of the non-bonded interaction, which is the main factor for the formation of the collapsed states. One can see this as well in Fig. 6(b), where the background color of the AC pseudo-phase is darker than the one of the UC pseudo-phase, which is due to the smaller end-to-end distance in this configuration.

For $\varepsilon = 2$ kcal/mol, two more local extrema in the derivatives of the end-to-end distance $\partial_T \overline{R}_{\mathrm{end}}$ and radius of gyration $\partial_T \overline{R}_{\mathrm{gyr}}$ can be found at $T \approx 210$ K and $T \approx 300$ K in Figs. 5(d) and 5(f). These come from the fact that with increasing ε at some point, the polymer-stripe interaction will become so important that the polymer adopts a stretched out configuration that is completely aligned with a stripe as discussed

above. In the case of the $m = 2$ substrate, this point is not reached for $\varepsilon \leq 2$ kcal/mol, but first signals of this transition appear in the histograms and in the form of these peaks, and it can be expected to find this transition for even higher values of ε.

B. Long chains with $N = 65$

In addition to the short chains with $N = 30$, long polymers of length $N = 65$ were studied. In order to acquire sufficient statistics for these long chains, it was necessary to increase the amount of update sweeps by a factor of five compared to the shorter chains. As such, the simulations were carried out with 5×10^7 sweeps (with thermalisation for 5×10^6 sweeps). On top of that, each system was simulated separately five times with different random number seeds. To compensate the increased data volume, measurements were done only every tenth sweep. Because of the autocorrelation of Markov chain Monte Carlo simulations, this does not decrease the effective statistics of the simulation.

The longer polymers exhibit several structural phases. The distinction between states where the polymer is unaligned with the stripes (U) and states where it is aligned (A) can be made again. Similar to the short polymers, one can also see compact states that resemble hairpins (C1) again. But because of the increased length of the polymer, many variations of compact states can occur. Most notably, a double-hairpin (C2) and similar densely packed circular configurations like spirals can be found. These two different compact pseudo-phases can be distinguished from each other by their respective end-to-end distances and radii of gyration. The end-to-end distance for the single-hairpin (C1) is very small, whereas it is longer for the double-hairpin (C2) because the ends of the chain are separated farther in this configuration. On the other hand, the double-hairpin features a very small radius of gyration because of the dense packing of the structure, and the single-hairpin has a relatively higher radius of gyration because it is not as compact as the double-hairpin. For the most part, the polymer exhibits a compact mixed phase, denoted by a C, which features both types of compact configurations. However, distinct structural phases of only one type of the compact structures can be found as well, especially in the regime of mostly aligned configurations.

The greatest difference to the case of the short chains is the lack of an extended phase in the studied temperature range. This is due to the fact that the longer chains have much more possibilities for the polymer to interact with itself to reduce its internal energy and, thus, compact configurations are more favorable for the long chains even at high temperatures. On top of that, the increased length also leads to more possibilities for the polymer to arrange itself in a compact configuration, which can be seen by the presence of different compact structures. Because of that, compact configurations are less suppressed by entropy than in the case of the shorter polymers.

To illustrate the different structural phases, simulation snapshots of representative states are displayed in Fig. 7. Again the snapshots are chosen to present somewhat ideal configurations that make the distinction most clear and may not represent

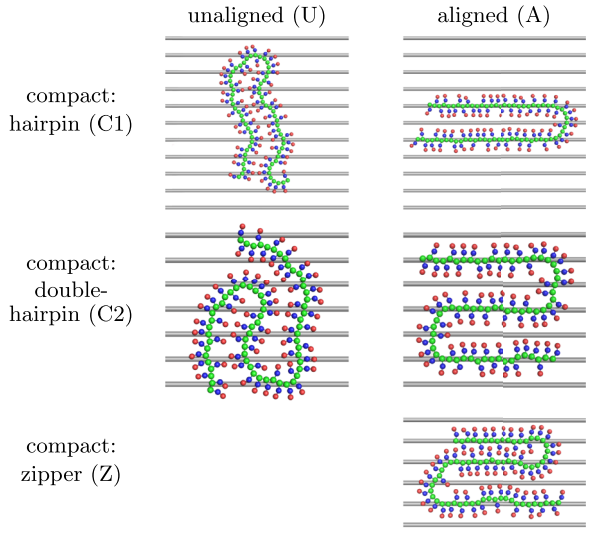

FIG. 7. Snapshots of coarse-grained P3HT polymers of length $N = 65$ in the different structural phases on a substrate with the stripe-distance parameter $m = 3.5$. Again the snapshots represent ideal examples of the different configurations and have been chosen to make the distinction between the structures clear.

the most typical configurations. Another distinct configuration is found in the simulations for the long polymers. It is characterized by a very dense hairpin and a high degree of order with interlocking side chains that resemble a zipper (Z). This finding will be discussed below. The derivatives of the measured observables with respect to temperature are shown in Fig. 8. The runaway behavior of the $\varepsilon = 1$ kcal/mol curves in the left column of Fig. 8 is caused by the zipper states and will be discussed below in more detail.

For the long polymers, substrates with a stripe-distance parameter of $m = 3.5$ were studied because of the analogy to the Au(001) surface again. The longer polymers show several conformational transitions that will be discussed here. The structural phase diagram is displayed in Fig. 9(a). Figure 9 only features maxima from positive regions of the derivatives of the observables and only minima from negative regions. This was done in order to make the structural phase diagrams clearer because a minimum in a positive region carries less significance to structural transitions than a maximum in a positive region. For example, a minimum in a positive region of the derivative of the end-to-end distance $\partial_T \overline{R}_{\text{end}}$ only means that the end-to-end distance is growing less severely—but it is still growing—whereas a maximum in a positive region signals a point where the growth is the fastest and something interesting might be happening to the polymer structure. As for the shorter polymers, the maxima of the substrate specific heat $c_{V,\text{sub}}$ show the transition from states where the long polymers try to be aligned with the substrate (A) to states where they are unaligned (U). With increasing ε, the transition temperature gets shifted higher, which is to be expected since more attractive stripes will dominate the polymer's behavior for longer while temperature is increased, which is also seen in the total specific heat c_V in Fig. 8(a). When comparing this phase diagram to the one for $N = 30$ in Fig. 6(a), one can see that the transition temperatures of the A ↔ U-transition are higher for the longer polymers. This is because a longer polymer has

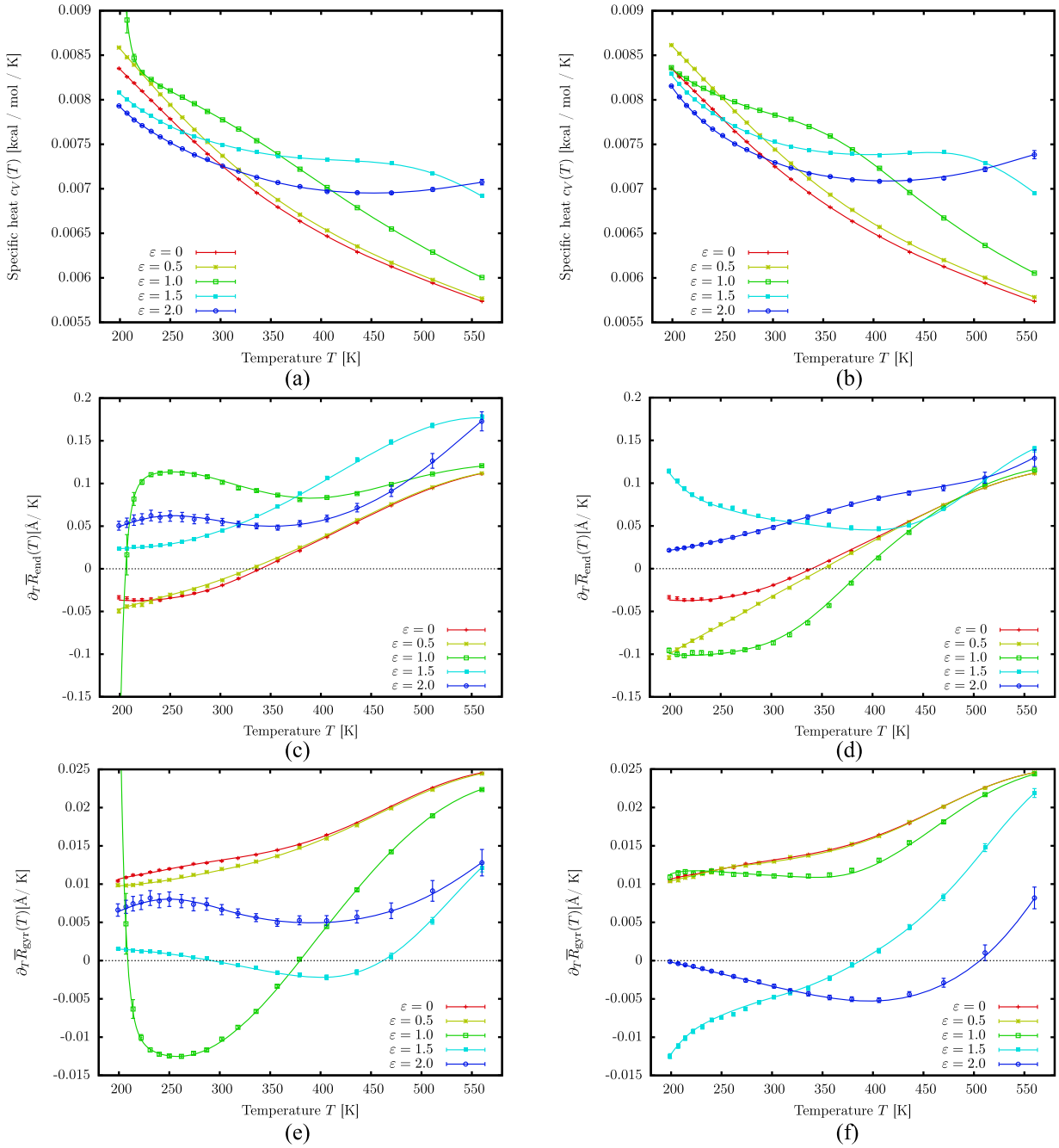

FIG. 8. Derivatives of the various observables for long polymers with $N = 65$ for distance parameter values of $m = 3.5$ [(a), (c), and (e)] and $m = 2$ [(b), (d), and (f)]. Shown are the total specific heat from both internal polymer and substrate interactions $c_V(T)$ [(a) and (b)] and the derivatives of the end-to-end distance $\partial_T \overline{R}_{\mathrm{end}}(T)$ [(c) and (d)] and radius of gyration $\partial_T \overline{R}_{\mathrm{end}}(T)$ [(e) and (f)] as functions of temperature T at different values of the interaction parameter ε in units of kcal/mol. The continuous lines are the result of the multiple-histogram reweighting.

more backbone particles to interact with the stripes. Therefore, the stripe interaction will be the dominant force at even higher temperatures compared to short polymers.

As discussed above, the long 2D polymers do not adopt an extended structural phase and, thus, no collapse transition with the maxima of the derivatives of the end-to-end distance and radius of gyration can be found in this temperature range. The compact structural phase (C) is made up of a mixture of single-hairpin (C1) as well as double-hairpin (C2) configurations. Interestingly though, it seems that in the range of not so attractive stripes with $\varepsilon \leq 0.375$ kcal/mol, the more compact and round C2 states are more prevalent at low temperatures (UC2). With increasing temperatures, the "compactness" of the compact states is lowered and more C1 states can be found. A sign of this behavior is found as minima in the derivative of the end-to-end distance $\partial_T \overline{R}_{\mathrm{end}}$ at $T \approx 220$ K at $\varepsilon = 0, \ldots, 0.375$ kcal/mol [see Fig. 8(c) for $\varepsilon = 0$ kcal/mol]. This is also reflected in the canonical diagrams of $\overline{R}_{\mathrm{end}}(T)$ and $\overline{R}_{\mathrm{gyr}}(T)$ in Fig. 10, where the radius of gyration is steadily increasing with increasing temperature, but the end-to-end distance is decreasing at first due to the lower end-to-end distance in the C1 states. Additionally, this is seen in the diagrams of $\partial_T \overline{R}_{\mathrm{end}}(T)$ and

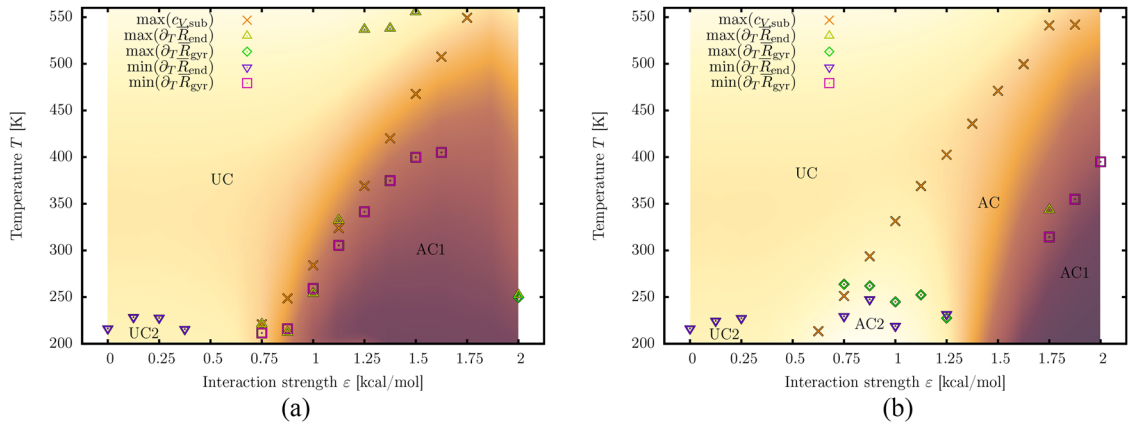

FIG. 9. Structural phase diagram for the polymers of length $N = 65$ and a stripe-distance parameter $m = 3.5$ (a) and $m = 2$ (b). The structural phases are distinguished as compact (C) with the two different types C1 and C2 and as aligned with the stripes of the substrate (A) or unaligned (U). The coloring of the background refers to the end-to-end distance $\overline{R}_{\mathrm{end}}$, where the lowest values are colored in dark purple and the highest values are colored in bright yellow. Both plots use the same range for background color, i.e., the same color refers to the same value in both plots. As such, one can make out several regions that correspond to the compact, single-hairpin (AC1, dark purple), compact, mixed (C, orange), and compact, double-hairpin (AC2, bright yellow) configurations.

$\partial_T \overline{R}_{\mathrm{gyr}}(T)$ in Figs. 8(c) and 8(e) for $\varepsilon = 0$ and $\varepsilon = 0.5$ kcal/mol, where the derivative of the radius of gyration is positive for all temperatures. The derivative of the end-to-end distance, on the other hand, is negative at first and only becomes positive around $T \approx 350$ K.

In the region of stronger polymer-stripe interactions $\varepsilon \geq 0.75$ kcal/mol at lower temperatures, the polymer is almost exclusively in the single-hairpin conformation (C1) such that one can actually speak of a distinct structural phase here. By increasing the temperature, the polymer again enters the mixed compact phase. This transition is marked by minima in $\partial_T \overline{R}_{\mathrm{gyr}}$ and some maxima in $\partial_T \overline{R}_{\mathrm{end}}$, which can also be found in Figs. 8(c) and 8(e) for $\varepsilon = 1$, 1.5 kcal/mol. The explanation for this can be found in the opposing behavior of the end-to-end distance and radius of gyration at this transition. The single-hairpin configuration has a very small end-to-end distance and large radius of gyration. By heating up the system, more C2 states enter the sample and lower the average radius of gyration while increasing the average end-to-end distance. For intermediate polymer-stripe interaction parameters 0.75 kcal/mol $\leq \varepsilon \leq$ 1.25 kcal/mol, the transitions A $\leftrightarrow$ U and C1 $\leftrightarrow$ C coincide because the stripe interaction is responsible for the formation of the C1 structures in the first place.

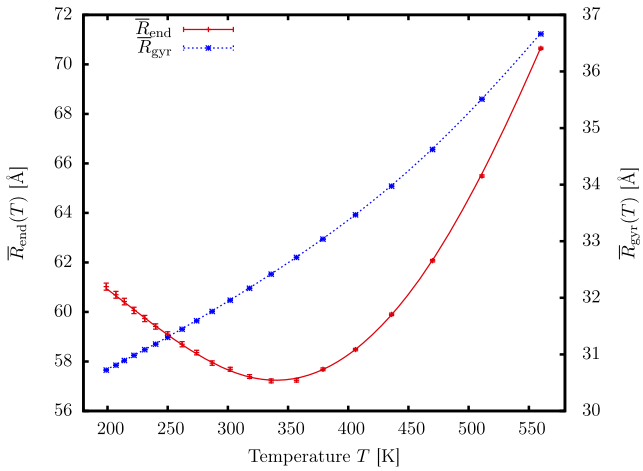

FIG. 10. End-to-end distance $\overline{R}_{\mathrm{end}}(T)$ (red, solid line) and radius of gyration $\overline{R}_{\mathrm{gyr}}(T)$ (blue, dashed line) for a 2D coarse-grained P3HT polymer of length $N = 65$ on a substrate with non-interacting stripes $\varepsilon = 0$. The lines are the result of the multiple-histogram reweighting.

In addition to the structural phases, we found another configuration with a high degree of order during the simulations of substrates with 0.875 kcal/mol $\leq \varepsilon \leq$ 1.25 kcal/mol at low temperatures $T \approx 200$ K. . .210 K. It is displayed in Fig. 7 as the compact "zipper" configuration (Z). The lower part of the polymer displays the usual aligned, compact behavior: The polymer aligns itself with stripes and forms a hairpin. In the normal case, two strands of the hairpin have a distance that is twice as large as the stripe distance, i.e., an unoccupied stripe lies between the two parts of the hairpin. However, the upper part of the polymer exhibits a highly ordered structure. Here the two strands of the hairpin are lying on neighboring stripes and are, thus, much more closely packed. To allow this structure to happen, the side chains on the inside of the hairpin are interwoven between the two strands. Only every third side chain is on the inside of the hairpin, the rest has to be flipped outside to make room for the side chains from the opposite strand. By this, they form a pattern that somewhat resembles a zipper. This also means that such a "zipper" state cannot occur in both strands of a double-hairpin because in one of the hairpins, there would not be enough space to form this interwoven structure. The complex structure, however, leads to the practical problem that it is not only improbable to enter these zipper states but also it is difficult for the Metropolis algorithm to leave them after they have been found. As a consequence, the simulations get thrown out of equilibrium once they attain a zipper state. This causes the runaway behavior of the $\varepsilon = 1$ kcal/mol curves in the left column of Fig. 8 at low temperatures. The parallel tempering did not prevent this since the zipper configurations are of very low energy and as such rarely get swapped up to higher temperatures. It could be expected to find these kinds of states in equilibrium at much lower temperatures after a supposed freezing transition. Similar structures have already been described in experimental studies for P3HT

crystals.[16,41,42] In Ref. 41, they find that the distance between two P3HT chains is D = 13.3 Å which is very similar to the stripe distance of D_{stripe} = 13.4 Å used here. The other studies find similar values. However, the experiments suggest a one-to-one interweaving not a one-to-two interweaving as seen here. This is likely to be an artifact of the coarse-grained model.

Both of the possibilities to arrange a hairpin in a Z state on a substrate with stripe-distance parameter m = 3.5 are not ideal. The large distance between the two strands in the bottom part is not ideal for the polymer because the "natural" distance of the hairpin-strands is actually a bit smaller. This can be seen in Fig. 7, where the unaligned states have much denser hairpins than the aligned states. On the other hand, the small distance in the upper part of the polymer is also far from ideal because it requires such a high amount of order to be feasible. This is also likely to be the reason why the polymers do not form an AC2 structural phase for this stripe distance as they do on the m = 2 substrate (as discussed below). This is similar to the case of the short polymers on substrates with m = 3.5, where compact structures are less prevalent in the aligned pseudo-phase. Because the stripe distance is too large for the internal attraction of the polymer to play the dominant role in the structure formation, less compact AC1 configurations are favored that minimize the substrate interaction energy (while still trying to minimize the polymer's internal energy to a certain degree, unlike the AS configurations of the shorter polymers).

Long polymers on a substrate with stripes that are m = 2 times the equilibrium distance of the P1-P1 bond apart from each other were studied as well. The phase diagram for this case can be seen in Fig. 9(b). There is a transition from states that are not aligned with the stripes (U) to states that are mostly aligned (A) which is marked by maxima in the substrate specific heat $c_{V,\text{sub}}$ as already seen in the case of m = 3.5. The region where the polymer is not aligned with the stripes is mostly unaffected by the change in the stripe distance because the stripe interaction is not the main driving force in this region anyway. Again, this can be seen in Fig. 8, where the curves for ε = 0, 0.5 kcal/mol are almost the same in the left (m = 3.5) and right (m = 2) columns. In the regime of only mildly attractive stripes, one can again see that at low temperatures, the polymer is mostly densely packed and adopts more roundish C2 states. A mixture of C1 and C2 states is found at higher temperatures as described above.

The region where the polymer is aligned with the stripes is different, however. In contrast to the case of m = 3.5, here a C2 structural phase can be identified in the region of medium interaction strengths (0.625 kcal/mol ≤ ε ≤ 1.25 kcal/mol) at low temperatures (AC2). The transition C2 ↔ C is marked by minima in $\partial_T \overline{R}_{\text{end}}$ and maxima in $\partial_T \overline{R}_{\text{gyr}}$, some of which are found in Figs. 8(d) and 8(f) for ε = 1 kcal/mol. Here the opposite of the C1 ↔ C transition from m = 3.5 is happening: The dominant C2 states have small radii of gyration and the ensemble average increases with temperature because more C1 states are attained and the general "extension" of the polymer is increased, whereas the end-to-end distances are relatively large for low temperatures and decrease with rising temperatures, when more C1 states enter the sample.

Similar to the m = 3.5 substrate, the substrates with a large interaction strength ε ≥ 1.625 kcal/mol exhibit an aligned, single-hairpin structural phase (AC1). There, the low temperatures are governed by C1 states and a transition into a mixed phase can be found, which is now marked by maxima in $\partial_T \overline{R}_{\text{end}}$ and minima in $\partial_T \overline{R}_{\text{gyr}}$. This is also reflected in Figs. 8(d) and 8(f). There one can see for ε = 1.5 kcal/mol and ε = 2 kcal/mol that the derivative of the end-to-end distance is positive over the whole temperature range, whereas the derivative of the radius of gyration is negative at first and only becomes positive for higher temperatures. As described above, the relatively linear single-hairpin configurations lead to a high radius of gyration in the ensemble average, which gets rapidly decreased once more C2 states enter the sample. The end-to-end distance, on the other hand, is small for low temperatures and then rises with increasing temperature for the same reasons. The remainder of the aligned region is characterized by a mixed compact structural phase (C). Here the polymers behave similar to the AC ↔ AS-transition region in the case of the short polymers on the m = 3.5 substrates.

IV. CONCLUSION

We implemented the coarse-grained model for P3HT by Huang *et al.* in two dimensions to investigate the structural phases of P3HT adsorbed on a substrate. We introduced an abstract potential to the substrate in order to find the effects of a stripe pattern. To generate the necessary data, we used parallel tempering as well as non-local update moves for the Metropolis steps of our Monte Carlo simulations. The data were evaluated using the direct multiple histogram reweighting by Fenwick and peaks in the canonical derivatives of the observables were used to produce structural phase diagrams of the system. We identified several distinct structural phases that are influenced by the shape and the attractiveness of the stripe pattern. The phases are governed by configurations such as hairpins, double-hairpins, and extended chains. A particularly intriguing structural motif is formed by interlocking side chains that form a "zipper"-like state. Similar configurations to the ones we found have already been described in experiments.[16,18,41,42] However, the resolution of the measurements is usually not high enough to make the behavior of the side chains clearly visible, which could be achieved in our study. Stripes which are closer together usually facilitate more compact configurations, whereas stripes that are further apart and in the regime of the surface reconstruction pattern of Au(001) tend to produce more stretched out configurations.

ACKNOWLEDGMENTS

We gratefully acknowledge support by the Deutsche Forschungsgemeinschaft (DFG) via the Sonderforschungsbereich/Transregio SFB/TRR 102 "Polymers under multiple constraints" (Project No. B04), which facilitated useful discussions with our experimental colleagues Wolf Widdra and Erik Schreck, né Kohl.

[1]T. Bogner, A. Degenhard, and F. Schmid, Phys. Rev. Lett. **93**, 268108 (2004).
[2]N. Gupta and A. Irbäck, J. Chem. Phys. **120**, 3983 (2004).
[3]J. J. Cerda and T. Sintes, Biophys. Chem. **115**, 277 (2005).
[4]Y. A. Kriksin, P. G. Khalatur, and A. R. Khokhlov, J. Chem. Phys. **122**, 114703 (2005).
[5]K. Sumithra and E. Straube, J. Chem. Phys. **125**, 154701 (2006).
[6]A. Swetnam and M. P. Allen, Phys. Rev. E **85**, 062901 (2012).
[7]M. Möddel, W. Janke, and M. Bachmann, Phys. Rev. Lett. **112**, 148303 (2014).
[8]B. Xu and S. Holdcroft, Macromolecules **26**, 4457 (1993).
[9]Z. Bao, A. Dodabalapur, and A. J. Lovinger, Appl. Phys. Lett. **69**, 4108 (1996).
[10]M. R. Andersson, O. Thomas, W. Mammo, M. Svensson, M. Theander, and O. Inganäs, J. Mater. Chem. **9**, 1933 (1999).
[11]B. W. Boudouris, V. Ho, L. H. Jimison, M. F. Toney, A. Salleo, and R. A. Segalman, Macromolecules **44**, 6653 (2011).
[12]J. M. Frost, F. Cheynis, S. M. Tuladhar, and J. Nelson, Nano Lett. **6**, 1674 (2006).
[13]M. Campoy-Quiles, T. Ferenczi, T. Agostinelli, P. G. Etchegoin, Y. Kim, T. D. Anthopoulos, P. N. Stavrinou, D. D. Bradley, and J. Nelson, Nat. Mater. **7**, 158 (2008).
[14]A. M. Ballantyne, L. Chen, J. Dane, T. Hammant, F. M. Braun, M. Heeney, W. Duffy, I. McCulloch, D. D. Bradley, and J. Nelson, Adv. Funct. Mater. **18**, 2373 (2008).
[15]Z.-Y. Yang, H.-M. Zhang, G.-B. Pan, and L.-J. Wan, ACS Nano **2**, 743 (2008).
[16]Y.-F. Liu, K. Krug, and Y.-L. Lee, Nanoscale **5**, 7936 (2013).
[17]S. Förster and W. Widdra, J. Chem. Phys. **141**, 054713 (2014).
[18]S. Förster, E. Kohl, M. Ivanov, J. Gross, W. Widdra, and W. Janke, J. Chem. Phys. **141**, 164701 (2014).
[19]D. M. Huang, R. Faller, K. Do, and A. J. Moulé, J. Chem. Theory Comput. **6**, 526 (2010).
[20]R. Hammer, A. Sander, S. Förster, A. Kiel, K. Meinel, and W. Widdra, Phys. Rev. B **90**, 035446 (2014).
[21]J. C. Slater, J. Chem. Phys. **41**, 3199 (1964).
[22]W. Janke, "Monte Carlo simulations in statistical physics—From basic principles to advanced applications," in *Order, Disorder and Criticality: Advanced Problems of Phase Transition Theory*, edited by Y. Holovatch (World Scientific, Singapore, 2012), Vol. 3, p. 93.
[23]D. P. Landau and K. Binder, *A Guide to Monte Carlo Simulations in Statistical Physics*, 4th ed. (Cambridge University Press, Cambridge, 2015).
[24]M. Newman and G. Barkema, *Monte Carlo Methods in Statistical Physics* (Oxford University Press, New York, 1999).
[25]N. Metropolis, A. W. Rosenbluth, M. N. Rosenbluth, A. H. Teller, and E. Teller, J. Chem. Phys. **21**, 1087 (1953).
[26]W. K. Hastings, Biometrika **57**, 97 (1970).
[27]R. H. Swendsen and J.-S. Wang, Phys. Rev. Lett. **57**, 2607 (1986).
[28]C. J. Geyer, "Markov chain Monte Carlo maximum likelihood," in *Computing Science and Statistics: Proceedings of the 23rd Symposium on the Interface*, edited by E. M. Keramidas and S. M. Kaufman (Interface Foundation, Fairfax, Virginia, 1991), p. 156.
[29]C. J. Geyer and E. A. Thompson, J. Am. Stat. Assoc. **90**, 909 (1995).
[30]K. Hukushima and K. Nemoto, J. Phys. Soc. Jpn. **65**, 1604 (1996).
[31]M. Lal, Mol. Phys. **17**, 57 (1969).
[32]N. Madras and A. D. Sokal, J. Stat. Phys. **50**, 109 (1988).
[33]F. T. Wall and F. Mandel, J. Chem. Phys. **63**, 4592 (1975).
[34]K. Kremer and K. Binder, Comput. Phys. Rep. **7**, 259 (1988).
[35]M. K. Fenwick, J. Chem. Phys. **129**, 125106 (2008).
[36]M. Möddel, W. Janke, and M. Bachmann, Macromolecules **44**, 9013 (2011).
[37]K. S. Austin, J. Zierenberg, and W. Janke, Macromolecules **50**, 4054 (2017).
[38]W. Janke, "Statistical analysis of simulations: Data correlations and error estimation," in *Proceedings of the Euro Winter School Quantum Simulations of Complex Many-Body Systems: From Theory to Algorithms*, NIC Series, Invited Lecture Notes, edited by J. Grotendorst, D. Marx, and A. Muramatsu (John von Neumann Institute for Computing, Jülich, 2002), Vol. 10, p. 423.
[39]D. P. Landau, Phys. Rev. B **13**, 2997 (1976).
[40]H. Arkın and W. Janke, J. Chem. Phys. **138**, 054904 (2013).
[41]E. Mena-Osteritz, A. Meyer, B. M. Langeveld-Voss, R. A. Janssen, E. Meijer, and P. Bäuerle, Angew. Chem., Int. Ed. **112**, 2791 (2000).
[42]Y. Han, Y. Guo, Y. Chang, Y. Geng, and Z. Su, Macromolecules **47**, 3708 (2014).